JOURNAL OF GEOPHYSICAL RESEARCH, VOL. 105, NO. A11, PAGES 25,247–25,263, NOVEMBER 1, 2000

Walén and variance analyses of high-speed flows observed by Wind in the midtail plasma sheet: Evidence for reconnection

Marit Øieroset, Tai D. Phan, and Robert P. Lin

Space Sciences Laboratory, University of California, Berkeley

Bengt U. Ö. Sonnerup

Dartmouth College, Hanover, New Hampshire

Abstract. We have analyzed 4 days of Wind observations of high-speed convective flows of up to ~800 km s^{-1} in the plasma sheet at $X_{GSE} \sim -60\ R_E$ during late March and early April 1999. Both earthward and tailward flows were observed. The high-speed flows had a duration of several hours, unlike the shorter-lasting (tens of minutes) bursty bulk flows, which are typically observed closer to the Earth. We have analyzed in detail a ~10 hour interval of high-speed flows detected during rather low geomagnetic activity and northward interplanetary magnetic field. Our analysis indicates that the fast flows are produced by magnetic reconnection and that the observed flow reversals are consistent with the passage of a reconnection X line. First, the results of the shear stress balance test (the Walén test) indicate that the flow in the deHoffmann-Teller frame, which is aligned with the magnetic field, has an average flow speed that is ~60% of the Alfvén speed, consistent with the presence of slow shocks in the magnetotail reconnection layer. Furthermore, the slope of the Walén regression line switches sign at the flow reversals, as expected from reconnection. Consistent with the passage of a reconnection X line, the magnetic field component normal to the neutral sheet also reverses sign at the flow reversals. For this event the tailward flowing plasma is hotter than the earthward flowing plasma, consistent with the two plasmas being magnetically disconnected. Our observations imply that quasi-steady reconnection can occur in the midmagnetotail region during periods of persistent northward interplanetary magnetic field.

1. Introduction

In the classic picture by *Dungey* [1961], reconnection occurs in the current layer between interplanetary and terrestrial magnetic field lines at the dayside magnetopause, as well as between oppositely directed field lines in the Earth's magnetic tail. The reconnected field exerts a magnetic tension force that accelerates plasma away from the reconnection site.

For reconnection at the dayside magnetopause the magnetic field strength on the magnetospheric side of the current layer is larger, and the plasma density is lower than on the magnetosheath side. *Levy et al.*'s [1964] asymmetric reconnection model is valid for such a case. A symmetric reconnection model describing conditions for tail reconnection, with equal plasma density, equal magnetic field strength, and antiparallel magnetic fields on the two sides of the current layer, was provided by *Petschek* [1964]. The main difference between these two models is that the Petschek reconnection predicts a pair of slow shocks while the simplest form of the Levy et al. model predicts that the pair of slow shocks is replaced by a rotational discontinuity and a slow expansion fan.

If the magnetopause is a rotational discontinuity, ideal MHD predicts that the accelerated flow is Alfvénic in the deHoffmann-Teller (HT) frame of reference. The HT frame is the reference frame in which the convective electric field is zero. Fast flows and the evidence for a rotational discontinuity at the dayside magnetopause were first reported by *Paschmann et al.* [1979] and *Sonnerup et al.* [1981]. They applied a shear stress balance test (later named the Walén test) to the observations of fast flows and showed that the flow was Alfvénic and hence consistent with reconnection.

To date, the shear stress balance test (the Walén test) has rarely been applied to high-speed flows in the magnetotail. Initial attempts of shear stress balance analysis of high-speed flows in the tail were made by *Richardson et al.* [1989]. Evidence for Petschek reconnection has been reported in the deep tail region ($-100 > X_{GSE} > -200$) in the form of observations of slow-mode shocks at the lobe–plasma sheet boundary [*Feldmann et al.*, 1984, 1985; *Saito et al.*, 1995; *Seon et al.*, 1996]. The evidence in those studies consisted of checking the Rankine-Hugoniot relations across the boundary. *Saito et al.* [1995] found that the Rankine-Hugoniot

Paper number 2000JA900075..
0148-0227/00/2000JA900075$09.00

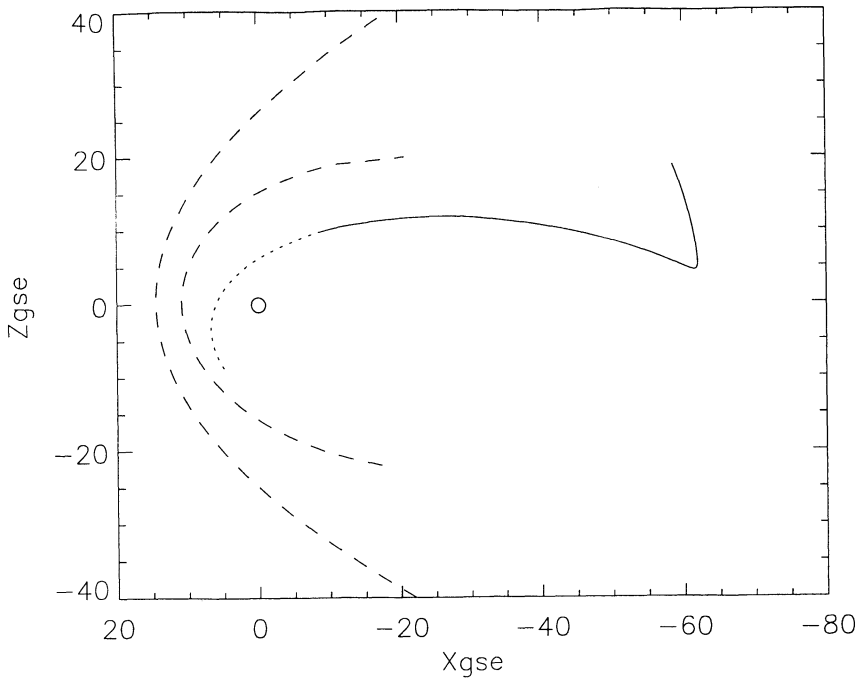

Figure 1. The Wind orbit (dotted and solid line) from 0000 UT on March 29 to 0000 UT on April 03, 1999, in the X-Z GSE plane. The statistical location of the magnetopause and the bow shock are marked with the dashed lines. The solid line marks the interval plotted in Plate 1.

condition was satisfied for only ~10% of the plasma sheet–lobe boundary crossings. In other studies, particle distributions indicative of reconnection were found [e.g., *Nagai et al.*, 1998].

In this study we report Wind observations of high-speed flows in the plasma sheet at $X_{GSE} \sim -60\ R_E$. We first perform a detailed quantitative comparison between the observed high-speed flows and the predictions from the Walén relation. Using variance analysis, we then show that the component of the magnetic field normal to the neutral sheet changes sign when the fast flow changes direction from earthward to tailward, consistent with the passage of a reconnection X line. Together, these findings provide strong evidence for the occurrence of reconnection in the midtail plasma sheet.

2. Observations

We use data from the Wind spacecraft. Plasma parameters are obtained from the three-dimensional "top hat" electrostatic ion analyzers, with energy range from 80 eV to 30 keV [*Lin et al.*, 1995]. The time resolution for the ion observations used in this study was 48 s (for some intervals, 96 s). The magnetic field data used in the present study are averaged over 48 s. Details of the magnetic field instrument are described by *Lepping et al.* [1995].

Figure 1 shows the Wind orbit in the X-Z GSE plane from 0000 UT on March 29 to 0000 UT on April 3, 1999. During this "lunar backflip" orbit, Wind spent more than 4 days in the magnetotail, moving antisunward to $X_{GSE} \sim -60\ R_E$, where lunar gravity was used to change its orbit. Plate 1 shows an overview of the Wind data obtained during these 4 days in the magnetotail. From top to bottom, plates 1a-1i show the ion density, parallel and perpendicular ion temperature, ion velocity, and magnetic field components as well as the spacecraft position in GSE coordinates. The spacecraft encountered alternately the low-density (<0.03 cm^{-3}) mantle/lobe plasma and the higher-density (0.05-0.3 cm^{-3}) plasma sheet (Plate 1a). High-speed flows were frequently observed when Wind was in the plasma sheet. These flows had durations of several hours. The main component of the

Table 1. Observations of High-Speed Flows by the Wind Spacecraft From March 30 to April 2, 1999

Interval Number	Fast Flow Interval	X_{GSE}	Maximum Positive	Maximum Negative	Type of Flow
1	March 30, 0314-0725	25-29	200	-50	beams
2	March 30, 1410-2017	33-40	500	-300	beams
3	March 31, 1558-0018 (+1 day)	50-55	800	-800	convective
4	April 1, 0432-1520	56-61	800	-800	convective
5	April 2, 1020-1818	61	800	-400	convective

high-speed flows was in the X direction, and both earthward and tailward flows were observed (see Plates 1c, 1d, and 1e). Overall, earthward flows occurred more often than tailward flows.

Table 1 summarizes the fast-flow observations. Five intervals (intervals 1-5) of fast flow, in both the earthward and tailward directions, can be distinguished in Plate 1. The first interval started on March 30 at 0314 UT, with Wind approximately 25 R_E downtail, and lasted for more than four hours. The earthward flow speed was less than 200 km s^{-1}, and the tailward speed was less than 50 km s^{-1} for this interval. The second interval occurred near 35 R_E downtail between 1410 and 2017 UT on the same day. The flow velocities were now significantly larger, with maxima of 500 km s^{-1} for the earthward flow and 300 km s^{-1} for the tailward flow. Even larger velocities were observed in the third interval, on March 31 between 1558 and 0018 UT. In this interval, comparable earthward and tailward velocities of up to 800 km s^{-1} were observed. The downtail distance was between 50 and 55 R_E. Similar velocities were observed between 56 and 61 R_E in the fourth interval, between 0432 and 1520 UT on April 1. The fifth interval of high-speed flows occurred on April 2 from 1020 to 1818 UT. In this interval, earthward velocities were still observed at up to 800 km s^{-1} while the tailward velocities had decreased to 400 km s^{-1}. This last interval of fast flows was observed near 61 R_E downtail.

Examination of the ion distributions reveals that the high-speed flows in intervals 1 and 2 consist of counterstreaming magnetic field-aligned ion beams. Thus the velocity moments do not adequately characterize the actual motion of the ions. These beams were detected when the spacecraft was in the high-latitude plasma sheet (10 nT< B_x <25 nT), i.e., far away from the neutral sheet.

The high-speed flows in intervals 3, 4, and 5, on the other hand, are true convective flows. Plate 2 shows four examples of two-dimensional cuts through the three-dimensional distributions observed in interval 4. The horizontal and vertical axes denote velocity components parallel and perpendicular to the magnetic field, respectively. The sunward direction is marked by the red line. Plates 2a and 2b show distributions obtained near the neutral sheet ($B_x \sim 0$), while Plates 2 c and 2d show two distributions obtained away from the neutral sheet. Plate 2a shows a distribution taken during earthward (sunward) flow at 0636 UT, while Plate 2b shows an ion distribution during tailward (antisunward) flow at 0934 UT. In both cases the ion distribution consists of a single population with bulk motion perpendicular to the magnetic field. The distribution in Plate 2a is moving in the sunward direction at a core speed of 386 km s^{-1}, while the distribution in Plate 2b is moving antisunward at a core speed of 598 km s^{-1}. The distributions obtained away from the neutral sheet (Plates 2c and 2d) have a component parallel to $\mathbf{B}$. However, these distributions still contain a component perpendicular to $\mathbf{B}$ and also consist of single populations. This type of convective single population is characteristic for the high-speed flows in intervals 3, 4, and 5.

For quantitative comparison with reconnection predictions we concentrate on the observations of high-speed flows seen in interval 4, at X_{GSE} ~60 R_E. Plate 3 shows a zoom-in of this interval from 0430 UT to 1500 UT on April 1, 1999. This interval is chosen because of the presence of uninterrupted high-speed flows for many hours and because Wind observed two high-speed convective flow reversals (at ~0756 and ~1015 UT) which indicate earthward and tailward passages of an X line.

3. Test of Walén Relation

Plate 3 shows the presence of earthward high-speed flows followed by tailward flows, then back to earthward flows. Magnetic reconnection in the magnetotail is a process that could account for such large plasma acceleration. In this section the reconnection hypothesis is tested using Walén analysis. The results of the analysis indicate that the transition from earthward to tailward flow is due to the passage of a reconnection X line.

Shear stress balance has been successfully tested on a number of high-speed flows observed at the dayside magnetopause [*Paschmann et al.*, 1979, 1986; *Sonnerup et al.*, 1981, 1987, 1995; *Gosling et al.*, 1986, 1990]. For a rotational discontinuity, ideal MHD predicts that the accelerated flow is Alfvénic in the deHoffmann-Teller (HT) frame of reference [*Sonnerup et al.*, 1987]. This condition is called the Walén condition and is expressed as

$$\mathbf{v} - \mathbf{V}_{HT} = \pm \frac{\mathbf{B}\sqrt{(1-\alpha)}}{\sqrt{\mu_0 \rho}}, \tag{1}$$

where $\mathbf{v}$ is the plasma velocity, $\mathbf{V}_{HT}$ is the deHoffmann-Teller velocity, $\mathbf{B}$ is the magnetic field, ρ is the total mass density, and $\alpha \equiv (p_{||} - p_{\perp})\mu_0/B^2$, where $p_{||}$ and $p_{\perp}$ are the plasma pressures parallel and perpendicular to $\mathbf{B}$. In the deHoffmann-Teller frame the electric field ideally vanishes.

Predictions similar to (1) exist for reconnection in the magnetotail, although tail reconnection layers do not include a rotational discontinuity. This is because reconnection in the tail involves symmetric conditions, with equal magnetic field magnitude and density on the two sides of the current sheet. In this case, the rotational discontinuity and the slow expansion fan that exist for dayside magnetopause reconnection [*Levy et al.*, 1964] are replaced by two standing, slow mode shocks [*Petschek*, 1964].

Under the assumption of isotropic pressure ($\alpha = 0$) the jump conditions across a slow-mode MHD shock lead to the following conclusions. When evaluated in the HT frame the Alfvén-Mach number, $M_{A1} = V_1\sqrt{\mu_0\rho/B_1}$, of the flow into the shock front is less than unity, except that it is equal to unity for the strongest slow-mode shock, in which the component of the magnetic field tangential to the shock front is switched off (a switch-off shock). Furthermore, the Alfvén-Mach number M_{A2} of the flow leaving the shock on its downstream side is such that $M_{A2} < M_{A1}$ [e.g., *Hau and Sonnerup*, 1989, Figure 1]. The actual value of M_{A2} depends on the shock strength, measured by M_{A1}, as well as on the upstream plasma β value ($\beta_1 = p_1 2\mu_0/B_1^2$), the angle θ_1 between the shock normal and the upstream magnetic

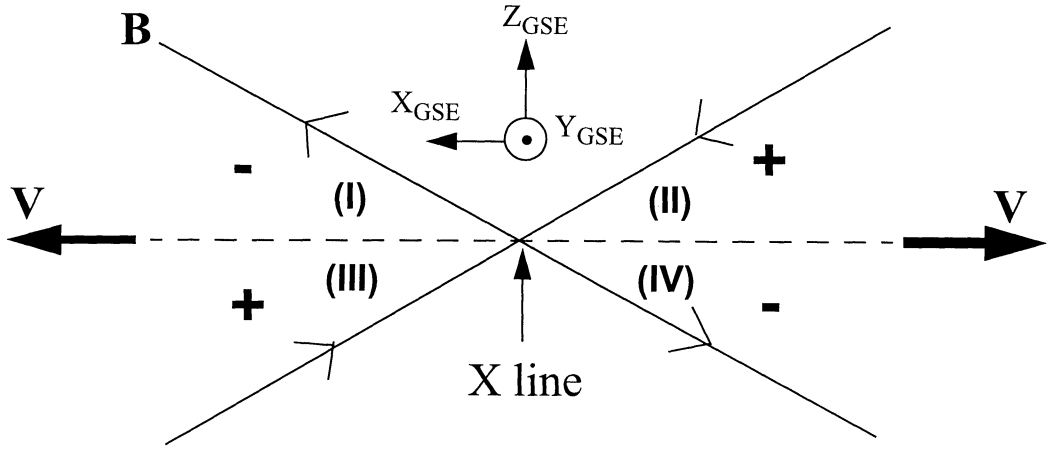

Figure 2. A schematic illustration of a reconnection configuration. The Earth is to the left of the figure. The dashed line marks the neutral sheet. The X line is perpendicular to the page. The sign of the Walén relation (equation (2)) is positive for segments III (earthward flow, Southern Hemisphere) and II (tailward flow, Northern Hemisphere) and negative for segments I (earthward flow, Northern Hemisphere) and IV (tailward flow, Southern Hemisphere).

field, and γ, the ratio of specific heats at constant pressure and constant volume. Within the shock front itself, assuming it has finite thickness, the Alfvén-Mach number is expected to decrease gradually from its upstream value M_{A1} to its downstream value M_{A2}. It follows that for a slow shock with $\alpha = 0$ the Walén relationship, equation (1), is replaced by

$$\mathbf{V} - \mathbf{V}_{\mathrm{HT}} = \pm M_A \frac{\mathbf{B}}{\sqrt{\mu_0 \rho}}, \tag{2}$$

where the local Alfvén-Mach number M_A varies from point to point but lies in the range $M_{A2} \leq M_A \leq M_{A1}$. The actual numerical range of M_A values depends on shock strength M_{A1} as well as on β_1, θ_1, and γ. For example, for a switch-off shock we have $M_{A1} = 1$ in the upstream region, and for angles θ_1 approaching 90°, such that $\cos^4\theta_1$ can be neglected compared to unity, we can show that

$$M_{A2} \simeq \sqrt{1 - \frac{1}{\gamma(1+\beta_1)}} \tag{3}$$

in the downstream region. For such a strong slow shock in the plasma having $\gamma = 5/3$, the value of M_{A2} would range from 0.63 for $\beta_1 = 0$ to 1.0 for $\beta_1 = \infty$. If the shock is weaker ($M_{A1} < 1$), the range of M_{A2} values is lowered correspondingly.

In a scatterplot of the components of $(\mathbf{v} - \mathbf{V}_{\mathrm{HT}})$ versus the corresponding components of Alfvén velocity $\mathbf{V}_{\mathrm{A}} = \mathbf{B}/(\mu_0\rho)^{1/2}$ for a slow-mode shock, one therefore expects a nonlinear regression curve. If the data are nevertheless fitted with a straight regression line, as will be done here, a regression line slope that may have a magnitude considerably less than unity should be expected.

The choice of plus or minus signs on the right-hand side of (2) depends on whether the flow is parallel (plus) or antiparallel (minus) to the magnetic field. This is illustrated in Figure 2, which shows a sketch in the x-z plane of reconnection in the magnetotail. The neutral sheet (here assumed to be in the x-y plane) is marked with the dashed line, and the Earth is to the left. The correlation between the flow velocity and the magnetic field (i.e., the sign in equation (2)) depends on the quadrant in which the observations are made. For observations in sections II and III, the flow and field are predicted to be correlated. In sections I and IV, they should be anticorrelated.

The HT frame for a set of plasma measurements can be found by finding the reference frame in which the mean square of the electric field is as small as possible. This mean square is given by [*Sonnerup et al.*, 1987]

$$\begin{aligned} D(\mathbf{V}) &= \frac{1}{M}\sum_{m=1}^{M} \left|\mathbf{E}'^{(m)}\right|^2 \\ &= \frac{1}{M}\sum_{m=1}^{M} \left|(\mathbf{v}^{(m)} - \mathbf{V}) \times \mathbf{B}^{(m)}\right|^2 \end{aligned} \tag{4}$$

for M measurements of the plasma velocity $\mathbf{V}^{(m)}$ and magnetic field $\mathbf{B}^{(m)}$, $m = 1, 2, ..., M$.

The velocity $\mathbf{V}$ for which D($\mathbf{V}$) is a minimum is the deHoffmann-Teller velocity, $\mathbf{V}_{\mathrm{HT}}$. The value of D_{HT}/D_0 is often used as a measure of the quality of the HT frame, where

$$\begin{aligned} D_{\mathrm{HT}} &= D(\mathbf{V})_{\min} \\ &= \frac{1}{M}\sum_{m=1}^{M} \left|(\mathbf{v}^{(m)} - \mathbf{V}_{\mathrm{HT}}) \times \mathbf{B}^{(m)}\right|^2, \end{aligned} \tag{5}$$

$$D_0 = \frac{1}{M}\sum_{m=1}^{M} \left|\mathbf{v}^{(m)} \times \mathbf{B}^{(m)}\right|^2. \tag{6}$$

For a good HT frame, D_{HT}/D_0 is small ($<< 1$). The quality of the HT frame is also evident when a single velocity

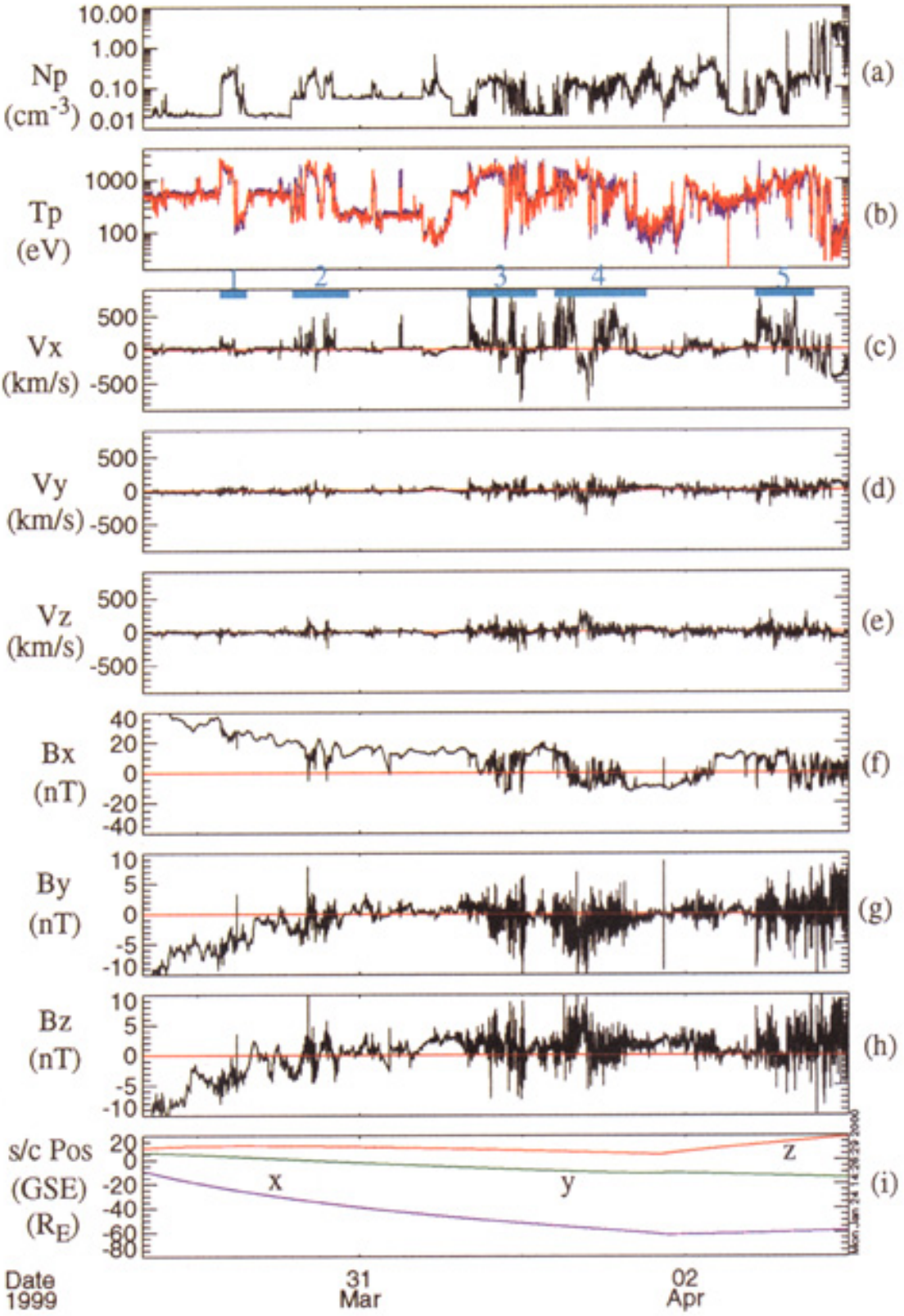

Plate 1. An overview of the Wind observations from March 29, 1600 UT to April 3, 0000 UT, 1999. Wind spent more than 4 days in the tail, traveling downstream to $X_{GSE} \sim 60\ R_E$. (a) The total ion density, (b) the parallel (blue) and perpendicular (red) ion temperatures, (c-e) the ion velocity components in GSE, (f-h) the magnetic field components in GSE, and (i) the orbit of the Wind spacecraft in GSE (x,blue; y,green; z,red).

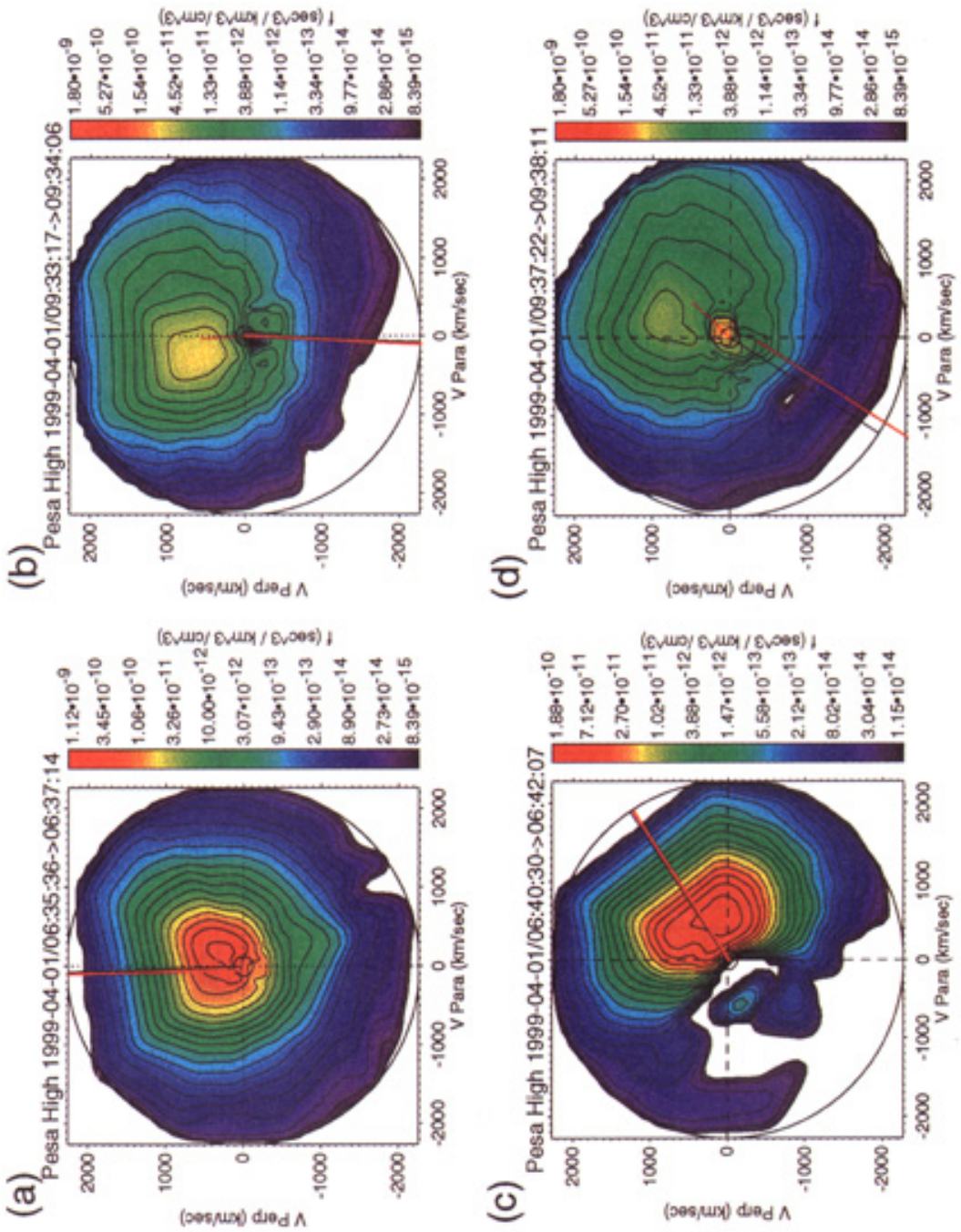

Plate 2. Two-dimensional cuts of the three-dimensional ion distributions obtained during the interval displayed in Plate 3. The two upper distributions are obtained near the neutral sheet, showing (a) a case of earthward high-speed flow and (b) a case of tailward high-speed flow. The two lower distributions are obtained away from the neutral sheet, again showing a case of (c) earthward and (d) tailward high-speed flow. All plots show a single convective population.

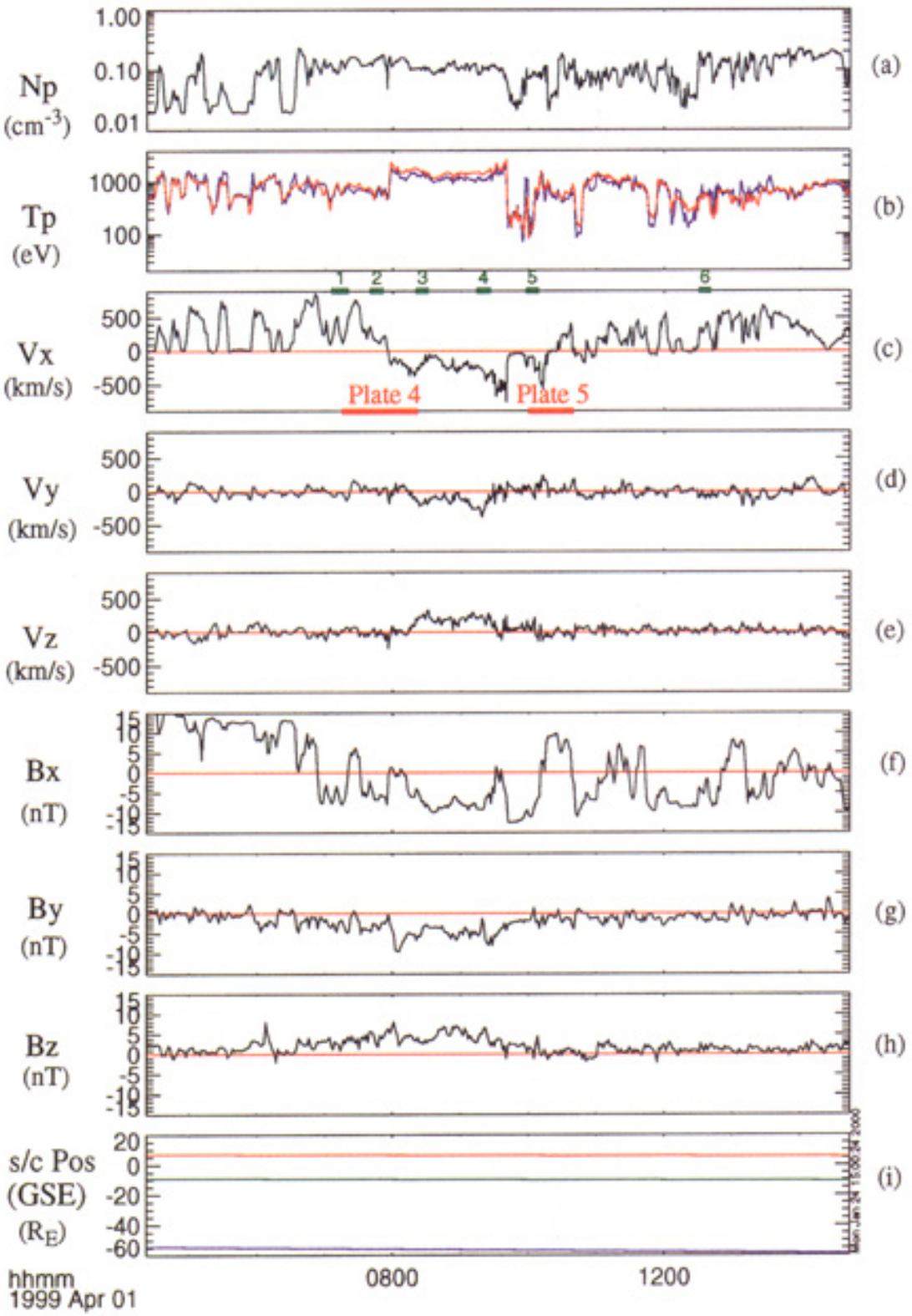

Plate 3. A zoom-in on the 0430 - 1500 UT interval on April 1, 1999, when Wind observed high-speed earthward flow followed by tailward flow and then followed by earthward fast flow again. The format is the same as in Plate 1. The intervals marked with green bars correspond to the six intervals (a - f) described in section 3.2. The intervals plotted in Plates 4 and 5 are also marked.

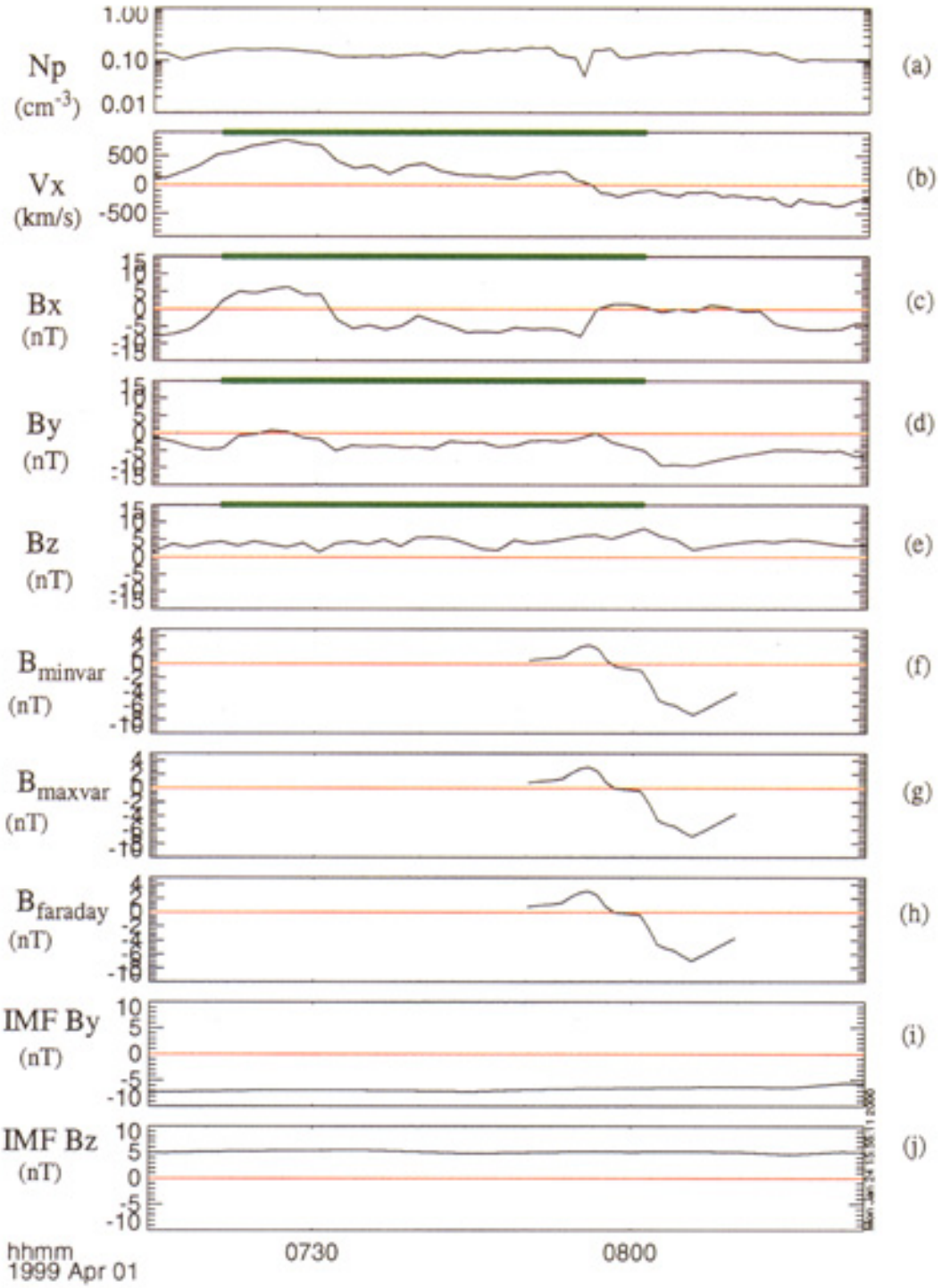

Plate 4. Seventy-five minutes of data near the transition from earthward to tailward high-speed flow at 0756 UT. The transition occurred at ~56 R_E downtail. The plasma density is shown in Plate 4a and the x component of the flow velocity is shown in Plate 4b. The magnetic field components are displayed in Plates 4c, 4d, and 4e, respectively. Plates 4f, 4g, and 4h show the components of the transformed magnetic field along the normal vector obtained by minimum variance analysis (B_{minvar}), maximum variance analysis (B_{maxvar}), and from minimization of the Faraday residue (B_{Faraday}), respectively. The normal components of the magnetic field obtained by all methods change sign as the flow changes direction from earthward to tailward. The variance analysis has been performed on the interval marked by the green bar. Time-shifted (by 66 min) interplanetary magnetic field (IMF) B_y and B_z components from the ACE spacecraft are shown in Plates 4i and 4j. Level 2 ACE magnetic field data were obtained from the ACE science center Web site at http://www.srl.caltech.edu/ACE/ASC/level2/.

Table 2. Summary of the Walén Analysis

Interval	Points	$\mathbf{V}_{HT}$ (V_x,V_y,V_z)	HT Slope	R_{HT}	D_{HT}/D_0	W Slope	R_W
a (0705:46-0720:26)	30	(530,60,-100)	1.02	0.97	0.03	0.64	0.92
b (0740:00-0751:49)	36	(370,110,-130)	1.07	0.94	0.08	0.59	0.96
c (0820:20-0831:45)	45	(-330,-310,270)	1.07	0.93	0.11	-0.33	-0.91
d (0914:08-0926:21)	48	(-590,-460,320)	1.05	0.96	0.08	-0.52	-0.98
e (0958:09-1008:44)	42	(-760,-60,160)	1.07	0.94	0.12	-0.83	-0.99
f (1230:37-1241:12)	42	(430,-30,-10)	1.09	0.94	0.05	0.54	0.89

The columns display the time interval, the number of data points, the deHoffmann-Teller velocity, the deHoffmann-Teller slope, the correlation coefficient, R_{HT}, for the deHoffmann-Teller relation, D_{HT}/D_0 (see definition in section 3), the Walén (W) slope, and the Walén correlation coefficient R_W.

$\mathbf{V}_{HT}$ is found for a data interval such that $-\mathbf{v}^{(m)} \times \mathbf{B}^{(m)} \approx -\mathbf{V}_{HT} \times \mathbf{B}^{(m)}$, where the superscript m denotes individual data points in the interval. In other words, a good correlation between the GSE components of $-\mathbf{v}^{(m)} \times \mathbf{B}^{(m)}$ and the corresponding components of $-\mathbf{V}_{HT} \times \mathbf{B}^{(m)}$ with a regression slope of $\sim$1 between these quantities indicates the existence of a good deHoffmann-Teller frame.

3.1. Procedure. We analyze six intervals (a - f) indicated by green bars in Plate 3. We first compute the deHoffmann-Teller velocity, $\mathbf{V}_{HT}$, for each interval using a method developed by *Sonnerup et al.* [1987]. The deHoffmann-Teller velocity is a combination of the field line motion tangential to the current layer and the current layer motion normal to itself. For our observations, $\mathbf{V}_{HT}$ is mainly in the sunward (x) or antisunward (-x) direction. The y and z components are associated with the current layer motion, i.e., the flapping of the tail, in addition to the reconnection flows. For all of these intervals, good deHoffmann-Teller frames were found.

With $\mathbf{V}_{HT}$ determined, we examine the flow velocity in the HT frame as a function of the Alfvén velocity (equation (2)). A good correlation between the flow and the field is essential for the reconnection interpretation. The magnitude of the slope of the regression line is expected to be below, and usually substantially below, unity. The sense of the correlation (i.e., the sign in equation (2)) provides an important consistency check on the reconnection interpretation (Figure 2).

3.2. Analysis. Table 2 summarizes the results of this section.

3.2.1. Interval a (0705:46-0730:26 UT): Figure 3a shows the result of the deHoffmann-Teller velocity determination for this earthward flow interval. A HT velocity of (530$\hat{x}$ + 60 $\hat{y}$ -100$\hat{z}$)$_{GSE}$ km s^{-1} is obtained. When $-\mathbf{v}^{(m)} \times \mathbf{B}^{(m)}$ is plotted against $-\mathbf{V}_{HT} \times \mathbf{B}^{(m)}$, the best fit of the data points has a slope (the HT slope) of +1.02 and a correlation coefficient of 0.97. Together with the value $D_{HT}/D_0 = 0.03$, they indicate the existence of a good deHoffmann-Teller frame. Since B_x was negative throughout this interval, the spacecraft should be in section III of Figure 2. Figure 3a also shows the scatterplot of each GSE x, y, z component of the flow velocity in the HT frame versus the Alfvén velocity. On average, the flow speed in the HT frame is $\sim$64% of the Alfvén speed, and the correlation coefficient between the two quantities is $R_W = 0.92$. The slope of the regression line is positive, consistent with the spacecraft being in section III.

3.2.2. Interval b (0740:00-0751:49 UT): A second interval in the earthward flow portion, but closer to the flow reversal, is chosen for analysis to demonstrate the consistency of the result. The spacecraft is still located in the Southern Hemisphere ($B_x < 0$). Figure 3b shows that a good deHoffmann-Teller frame exists for this interval, with $\mathbf{V}_{HT}$ = (370$\hat{x}$ + 110 $\hat{y}$ -130$\hat{z}$)$_{GSE}$ km s^{-1}. The flow velocity in the HT frame is again well correlated with the Alfvén velocity (see also Table 2). The slope of the regression line is positive, again consistent with the spacecraft being in section III. On average, the flow speed is 59% of the Alfvén speed for this interval.

3.2.3. Interval c (0820:20-0831:45 UT): During this interval of tailward flow the flow velocity was rather small ($|V_x| < 100$ km s^{-1} typically). A good deHoffmann-Teller frame is found, with an HT slope of 1.07, a correlation of 0.93 (Figure 3c), and $D_{HT}/D_0 = 0.11$. The deHoffmann-Teller velocity has comparable components in all directions: $\mathbf{V}_{HT}$ = (-330$\hat{x}$ - 310 $\hat{y}$ + 270$\hat{z}$)$_{GSE}$ km s^{-1}. The correlation coefficient between ($\mathbf{v} - \mathbf{V}_{HT}$) and $\mathbf{V}_A$ is $R_W = -0.91$; the negative slope is consistent with the spacecraft being in section IV. However, the flow speed in the HT frame is only 33% of the Alfvén speed (Figure 3c).

3.2.4. Interval d (0914:08-0926:21 UT): For this interval of tailward flow the flow velocity is larger ($V_x \sim -300$ km s^{-1}). The spacecraft is still located in the Southern Hemisphere during this interval. As shown in Figure 3d, a good deHoffmann-Teller frame is found: ($\mathbf{v} - \mathbf{V}_{HT}$) and $\mathbf{V}_A$ are well correlated ($R_W = -0.98$), and the flow speed is 52% of the Alfvén speed. The negative slope is consistent with the spacecraft being in quadrant IV of the reconnection configuration (Figure 2).

3.2.5. Interval e (0958:09-1008:44 UT): In this interval, where the spacecraft remains in the Southern Hemisphere ($B_x < 0$), the tailward flow speed is still larger ($V_x \sim$-500 km s^{-1}). A good HT frame is found (Figure 3e). The corresponding deHoffmann-Teller velocity is $\mathbf{V}_{HT}$ = (-760$\hat{x}$ - 60$\hat{y}$ + 160$\hat{z}$)$_{GSE}$ (Table 2), which also has a large tailward component. The correlation between ($\mathbf{v} - \mathbf{V}_{HT}$)

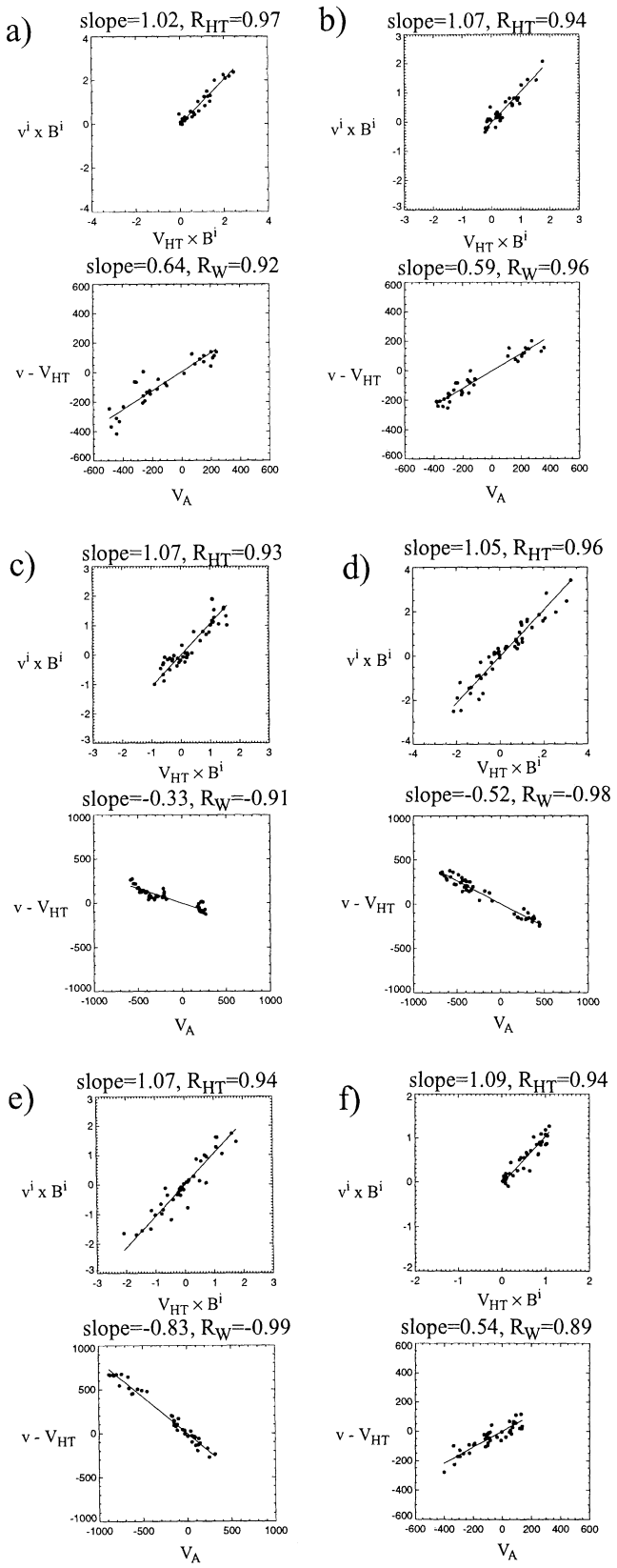

Figure 3. Results from deHoffmann-Teller and Walén analysis performed on the six intervals (a - f) marked on Plate 3. The upper plots of figures 3a - f show $\mathbf{V} \times \mathbf{B}$ versus $\mathbf{V}_{HT} \times \mathbf{B}$, while the lower plots show the velocity in the deHoffmann-Teller frame versus the Alfvén speed. The results of the analysis are summarized in Table 2.

and $\mathbf{V}_A$ is again good ($R_W = -0.99$), with a negative slope of -0.83 (Figure 3e). This is again consistent with the prediction of Figure 2 for section IV.

3.2.6. Interval f (1230:37-1241:12 UT): In this interval of earthward flow, following the tailward flows in intervals 3, 4, and 5, the spacecraft should be in section III (Figure 2). A good HT frame was found, and the slope of the Walén relation has now changed back to positive (Figure 3f), as expected in section III.

3.3. Summary of Walén test. We have analyzed six time intervals (a - f) where good HT frames were found, i.e., where the flow in the HT frame was well aligned with the magnetic field. For all cases, all three (GSE) components of the flow velocity in the HT frame were found to be linearly correlated with the corresponding Alfvén velocity components, and the flow speeds in the HT frame were almost exclusively sub-Alfvénic. With the exception of one event (interval c) the plasma flow speed in the HT frame was at least 52% of the Alfvén speed. As discussed earlier in this section, sub-Alfvénic flow is expected downstream of a slow shock [*Hau and Sonnerup*, 1989]. We have not performed tests of the slow-mode Rankine-Hugoniot (jump) conditions because the Wind plasma measurements in the low-density lobe region are not sufficiently accurate for such tests. Also, the MHD slow-shock jump conditions may not be applicable in a collisionless plasma when the shock width is comparable to the entire current layer, which is probably the case here. However, although the shock jump conditions have not been checked in quantitative detail, the observed range of Alfvén-Mach numbers is reasonable. The most significant feature of our results, however, is the fact that the sign of the slope of the Walén regression line (the W slope) varies with the sense of the high-speed flow and the location of the spacecraft relative to the neutral sheet, as predicted by the simple reconnection picture in Figure 2. Such a systematic relationship between the direction of the high-speed flow and the sign of the Walén slope is unlikely to be the result of random Alfvén or slow-mode wave propagation in the magnetotail.

To further demonstrate that the six events described in sections 3.2.1.–3.2.6. are not "unusually good" events, we now perform the same analysis as before, but this time for the entire ~10 hour interval shown in Figure 3, using a sliding window of 12 min duration. The increment between each 12 min window is one data point (~ 50 s). This results in a total of 612 intervals for the analysis. The results are shown in Figure 4. The HT slope and correlation coefficient for each of the 612 intervals are shown in Figures 4b and 4c, respectively. Figure 4d displays D_{HT}/D_0.

For a good HT frame the HT slope and the HT correlation coefficient R_{HT} must be near unity and $D_{HT}/D_0 << 1$ [*Sonnerup et al.*, 1987]. It can be shown that $R_{HT} = 1 - D_{HT}/D_0$ [*Khrabrov and Sonnerup*, 1998a]. Figure 5 shows that the HT slope and R_{HT} are intimately related, as expected: Good HT slope (S_{HT}) cases ($S_{HT} \approx 1$) tend to have excellent R_{HT} (i.e., small D_{HT}/D_0).

It is evident from Figures 4b, 4c, and 4d that good HT frames do not exist in many intervals. To proceed to the

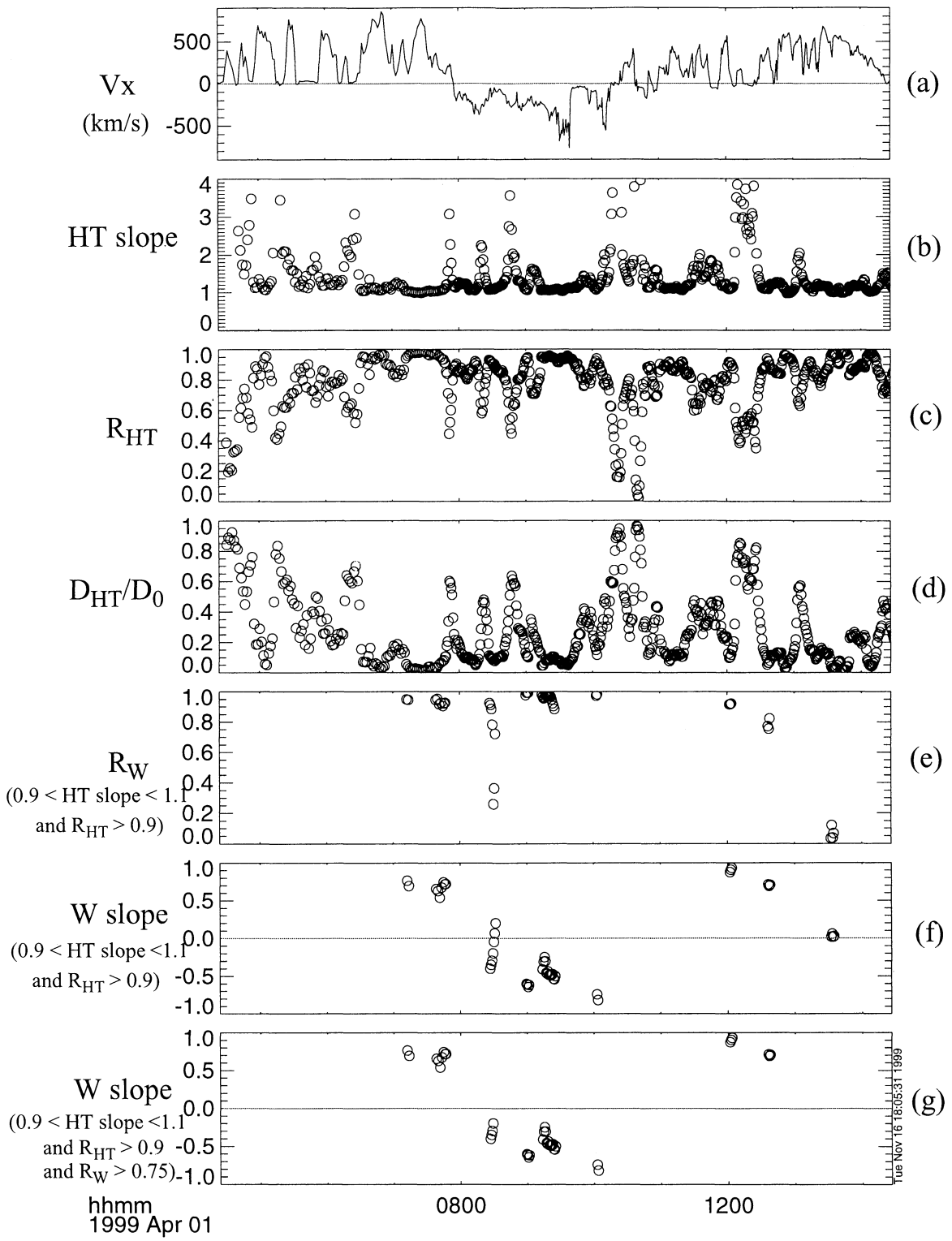

Figure 4. Sliding window HT and Walén analysis on the 10 hour interval of earthward and tailward high-speed flow. Figure 4a shows the V_x component. Figures 4b - d display the HT slope, S_{HT}, the HT correlation coefficient R_{HT}, and D_{HT}/D_0 for all 612 twelve minute intervals. Figures 4e and 4f show the Walén correlation coefficient R_W and the Walén slope (W slope) for 47 intervals with $B_x < 0$, with $0.9 < S_{\mathrm{HT}} < 1.1$, and with $R_{\mathrm{HT}} > 0.9$. Figure 4g shows 40 intervals having the W slope satisfy the additional selection criteria of $R_W > 0.75$.

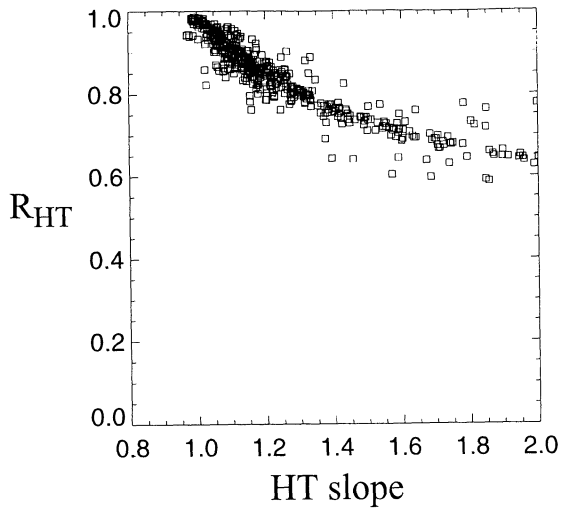

Figure 5. HT correlation coefficient versus HT slope. The 612 twelve minute intervals from the sliding window HT and Walén analysis in Figure 4 have been used.

Walén test, we impose the strict condition of a HT slope between 0.9 and 1.1 and $R_{\rm HT} > 0.9$ in order to select only cases with acceptable HT frames. The existence of a good HT frame does not imply reconnection, but it is a necessary condition for use of the Walén test which assumes time-stationary reconnection structures.

The Walén test should be performed on data on one side of the neutral sheet only (compare Figure 2). To simplify the analysis, we select only intervals when the spacecraft remains in the Southern Hemisphere ($B_x > 0$). Figures 4e and 4f display the Walén correlation coefficient R_W and the Walén regression line (the W slope) for the 47 intervals which satisfy the above selection criteria. By comparison with Figure 4a the main trend is seen to be that the Walén slope is positive for earthward flow and negative for tailward flow. A few data points (near 0830 UT and 1330 UT) do not follow this trend. However, these are cases with poor Walén correlations (R_W). For the 40 intervals with R_W better than 0.75 there are no more exceptions to the trend (Figure 4g). The average flow speed for these 40 intervals is 57% of the Alfvén speed.

The relationship between the sense of the Walén slope and the flow direction is nontrivial. Its agreement with the simple picture in Figure 2 provides strong evidence for reconnection.

4. Variance Analyses

In this section, we perform another consistency check on the reconnection interpretation, namely the sense of the magnetic field component normal to the neutral sheet (B_n) and its reversal at the passage of an X line (see Figure 2). In other words, with the normal vector **n** due north, B_n is expected to be positive in sections I and III and negative in sections II and IV with a switch of sign at the earthward-to-tailward and tailward-to-earthward flow reversals.

For a simple situation when the neutral sheet lies in the equatorial (x-y) plane, the neutral sheet normal is oriented in the $\hat{z}$ direction. However, for a neutral sheet that is tilted relative to the equatorial plane the true normal needs to be determined.

4.1. First Flow Reversal

Plate 4 shows the transition from earthward to tailward flow at ~0756 UT on April 1 (see also Figure 3). The plasma density, the x component of the velocity, and the three magnetic field components are shown in Plates 4a-4e. The transition from earthward to tailward flow occurred at ~56 R_E downstream. There is no change of sign in B_z at the flow reversal. We now show that this is due to a significant tilt of the neutral sheet.

The neutral sheet normal can be determined by a variety of methods. Here we employ three independent methods to ensure that the normal vectors obtained by these methods are in agreement with each other: (1) minimum variance of the magnetic field [*Sonnerup and Cahill*, 1967], (2) maximum variance of the electric field [*Sonnerup et al.*, 1987, 1990], and (3) minimization of the Faraday residue [*Terasawa et al.*, 1996; *Kawano and Higuchi*, 1996; *Khrabrov and Sonnerup*, 1998b]. Table 3 gives a summary of the normal vectors and eigenvalues obtained by the three methods.

For the analysis we select the 0721-0801 UT interval indicated by the green bar in Plate 4. This interval corresponds mainly to the earthward flow portion of the event. The computed normal vector for this interval corresponds to the average orientation of the entire tail current sheet. Once the neutral sheet normal is computed, the magnetic field component normal to the neutral sheet is obtained by projecting the magnetic field vectors onto the normal vector. The projection is done for an interval extending further into the tailward flow region. Thus the results are only valid if the neutral sheet normal does not vary appreciably throughout these times. In section 4.1.4 we perform the same analysis but on the tailward flow portion of the event (0805-0840 UT) to demonstrate that the neutral sheet normal does not change significantly during the latter portion of the event.

4.1.1. Minimum variance of B. Analysis of the 0721-0801 UT interval gives the minimum variance normal vector $\mathbf{n}_{\rm minvar}$ = (-0.149$\hat{x}$, 0.887$\hat{y}$, 0.438$\hat{z}$). This vector lies mainly in the y-z (GSE) plane. The positive $\hat{y}$ component of the normal corresponds to a large neutral sheet tilt of 64° relative to the GSE equatorial plane. The eigenvalues corresponding to the maximum, intermediate, and minimum variances are $e_i = 18.5$, $e_j = 2.20$, and $e_k = 1.40$, respectively. The separation between e_j and e_k is small ($e_j/e_k = 1.6$), indicating that the minimum variance direction (and hence the normal vector) is not well determined in this case.

4.1.2. Maximum variance of E. It has been found that the maximum variance analysis often gives a robust prediction of the normal vector even in those cases where minimum variance analysis on **B** gives $e_j \simeq e_k$ and therefore

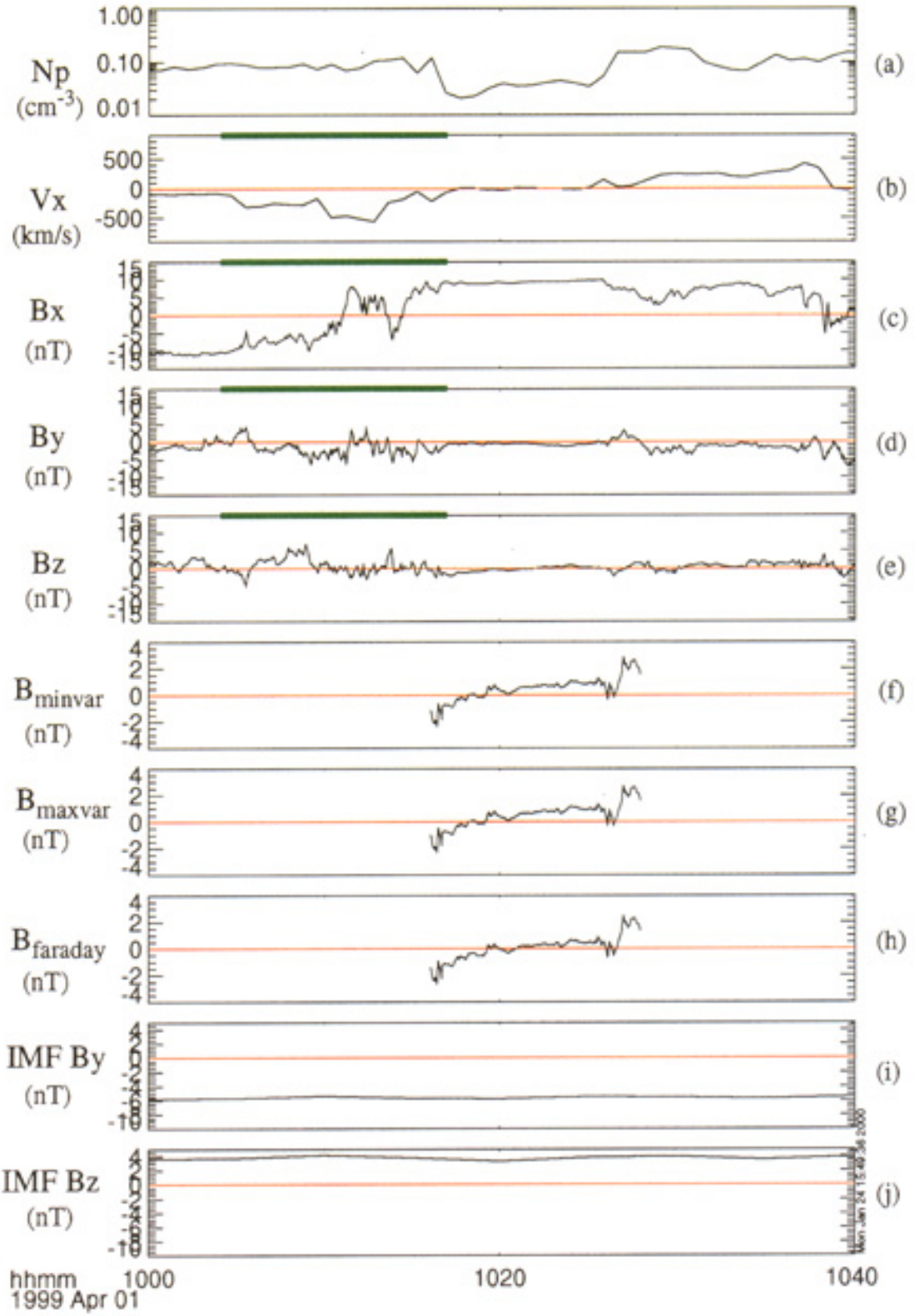

Plate 5. Forty minutes of data near the transition from tailward to earthward high-speed flow (the x component of the flow velocity is shown in Plate 5b at ~1015 UT. The transition occurred at ~57 R_E downtail. The format is the same as in Plate 4. The normal components of the magnetic field obtained by all methods change sign as the flow changes direction from tailward to earthward. The variance analysis has been performed on the interval marked by the green bar.

Table 3. Eigenvalues and Normal Vectors (GSE Components) Obtained by Minimum Variance Analysis (Minvar), Maximum Variance Analysis (Maxvar), and Minimization of the Faraday Residue (Faraday) for the 0721-0801 UT and the 1004 -1017 UT Intervals on April 1, 1999

Method	Eigenvalues (e_i, e_j, e_k)	Normal Vector (n_x, n_y, n_z)
	0721 - 0801 UT	
minvar	(18.5, 2.20, 1.40)	(-0.149, 0.887, 0.438)
maxvar	(1.37, 0.183, 0.0284)	(-0.150, 0.860, 0.488)
faraday	(1.55, 1.40, 0.210)	(-0.146, 0.858, 0.492)
	1004 - 1017 UT	
minvar	(42.3, 6.15, 2.16)	(0.115, 0.649, 0.752)
maxvar	(2.38, 0.373, 0.0366)	(0.118, 0.601, 0.790)
faraday	(2.59, 2.01, 0.384)	(0.0712, 0.638, 0.767)

fails to produce a reliable normal [*Sonnerup et al.*, 1987, 1990]. In the calculations presented here, the convective electric field ($-\mathbf{v} \times \mathbf{B}$) is used as a proxy for the total electric field. The normal vector from maximum variance analysis for this time interval is $\mathbf{n}_{\mathrm{maxvar}}$ = (-0.150$\hat{x}$, 0.860$\hat{y}$, 0.488$\hat{z}$). This corresponds to a tilt of 61° relative to the GSE equatorial plane. The eigenvalues corresponding to the maximum, intermediate, and minimum variance of the convective electric field are $e_i = 1.37, e_j = 0.183$, and $e_k = 0.0284$. The separation between the maximum and intermediate eigenvalues is large ($e_i/e_j > 7$), indicating that the normal is better determined by this method.

4.1.3. Minimization of the Faraday residue. A third method for finding the normal vector is by minimization of the Faraday residue. Employing the analytical method of *Khrabrov and Sonnerup* [1998b], one obtains, for the same interval as before, a normal vector of $\mathbf{n}_{\mathrm{Faraday}}$ = (-0.146$\hat{x}$, 0.858$\hat{y}$, 0.492$\hat{z}$). This corresponds to a tilt of the neutral sheet of 61° relative to the GSE equatorial plane. The eigenvalues in this case are $e_i = 1.55, e_j = 1.40$, and $e_k = 0.210$. Since the eigenvalues corresponding to the minimum and intermediate variance are well separated ($e_j/e_k > 6$), the minimum variance direction (i.e., the normal direction) is reasonably well defined.

4.1.4. Summary of variance analysis. We have obtained normal vectors from the three analysis methods. The normals obtained from the maximum variance of the electric field and from minimizing the Faraday residue agree to within 0.3°, whereas the normal from the minimum variance analysis of the magnetic field differs from the other two by 3°. This should not be surprising because, as pointed out in section 4.1.1, the minimum variance of **B** is less well defined. We conclude therefore that the true normal of the neutral sheet is better represented by $\mathbf{n}_{\mathrm{maxvar}}$ and $\mathbf{n}_{\mathrm{Faraday}}$.

Plates 4f-4h display the magnetic field component along the three normals just determined. These components change sign from positive to negative approximately when the fast flows change direction from earthward to tailward, consistent with crossing of a reconnection X line. Note that this qualitative agreement is true even when using the less accurate $\mathbf{n}_{\mathrm{minvar}}$. This indicates that the reversal of the normal magnetic field is a rather robust result. That the reversal of B_n did not coincide precisely with the flow reversal, but occurred ~2 min later, indicates that the X line was locally unfrozen from the plasma in which it was embedded so that its instantaneous location did not have to be the same as that of the reversal of V_x. Figure 6 shows a possible trajectory (trajectory 1) in the region near an X line for this flow reversal event.

To confirm the stability of the neutral sheet normal, we have also performed the variance analyses on an interval of tailward flow (0805-0840 UT) following the earthward flow. The neutral sheet normal in this case is tilted 43° relative to the equatorial plane in the same sense as that during the earthward flow portion.

4.1.5. Neutral sheet tilt and IMF B_y. Our analysis suggests that the neutral sheet tilt of 61° was stable for at

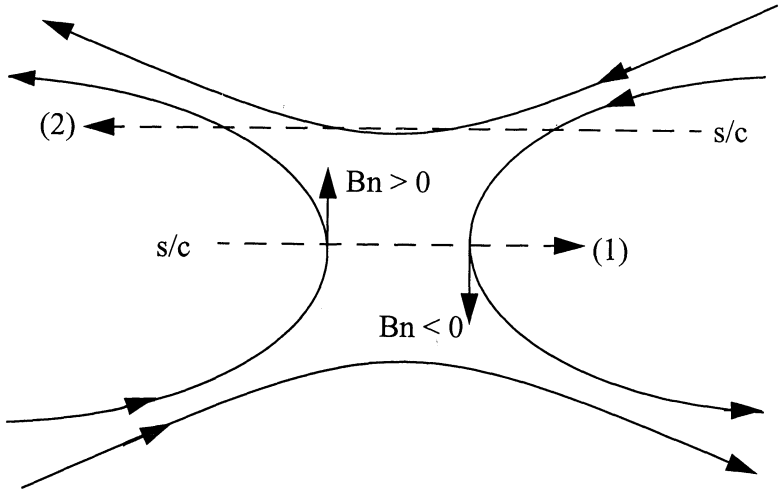

Figure 6. A schematic illustration of the magnetic field near an X line. The possible Wind trajectories for the earthward-to-tailward (trajectory 1) and the tailward-to-earthward (trajectory 2) flow reversals in Plates 4 and 5, respectively, are shown.

least 40 min. Here we investigate whether this substantial tilt could be due to effects associated with IMF B_y, as predicted by *Cowley* [1981].

The IMF B_y and B_z components observed by the ACE spacecraft are shown in Plates 4i and 4j. The ACE observations have been time-shifted by 66 min to take into account the solar wind convection from $X = 220\ R_E$ to $X = -60\ R_E$ at 440 km s^{-1}. It is seen that the IMF B_y component was persistently negative and large while the B_z component was positive but smaller throughout the interval chosen for variance analysis (marked by the green bar in Plate 4). For IMF $B_y < 0$, field lines reconnected on the dayside are added to the northern lobe predominantly on the dusk side and to the southern lobe on the dawn side [*Cowley*, 1981; *Sibeck et al.*, 1985; *Maezawa et al.* 1997]. This would result in a duskward tilt of the northward pointing neutral sheet normal, consistent with the results of our analysis. The steadiness of the IMF B_y component is also consistent with a persistent tilt of the neutral sheet.

The sense of the neutral sheet tilt is also consistent with the Z_{GSE} location where Wind encountered the neutral sheet. At 0756 UT, near the flow reversal, the spacecraft encountered the neutral sheet at $(x, y, z)_{GSE} = (-56, -9.7, 6.5)R_E$. Although the sense is correct ($Z_{GSE} > 0$), the current sheet tilt would only be 34° if one were to assume the center of the current sheet ($Y_{GSE} = 0$) to be "anchored" in the equatorial plane. However, at $X_{GSE} = -56\ R_E$, the entire neutral sheet could be displaced (offset) along the Z_{GSE} direction. The Z location of the neutral sheet at 60 R_E is likely to be associated with the flapping of the tail, as evident by variations in the B_x component.

4.2. Second Flow Reversal

The variance analyses described in section 4.1 have been applied to the second flow reversal near 1020 UT (Plate 5). In this case the high-speed flow changed from tailward to earthward, and the transition was not as sudden as in the previous example. The spacecraft entered a low-density region as the transition in flow direction took place.

The eigenvalues and normal vectors obtained by the three methods described in sections 4.1.1.–4.1.3 are summarized in Table 3. As in the previous case, the normal direction is less well determined by the minimum variance analysis because the eigenvalues e_j and e_k are not well separated, while the normal vectors from maximum variance and the Faraday residue technique are well determined. However, all three methods produce normal vectors which agree within 3.7°. The results of the analysis showing the normal components across the flow reversal obtained by the three different methods are shown in Plates 5f-5h. The three methods give qualitatively similar results.

The normal component (all three methods give similar normal components) changes sign from negative to positive across the flow reversal, consistent with crossing a reconnection X line. However, the transition between $B_n < 0$ and $B_n > 0$ is much more gradual than in the previous flow reversal case (Plate 4). In fact, the normal component of the magnetic field as well as the flow speed are close to zero for the interval when the spacecraft encountered a low-density region (1017-1026 UT). All these features are consistent with the spacecraft crossing the reconnection layer at higher latitudes, i.e., at some distance north of the X line itself, as illustrated in Figure 6, trajectory 2. Along this trajectory the spacecraft traverses the inflow region of reconnection where B_n is small and the flow speed is low. The lower density detected in this region also supports this simple scenario because the plasma in the high-speed flow (outflow) region is expected to be denser than the inflow plasma because of the compression across the slow shock. The low-density inflow region, sampled in interval 1017-1026 UT, might be either the lobe/mantle or the plasma sheet itself.

The neutral sheet tilt for the second flow reversal was ~40°, which is less than the 61° tilt found for the first flow reversal more than 2 hours earlier. However, a neutral sheet tilt of 40° is still substantial and still consistent with a large negative IMF B_y. As can be seen in Plates 6i and 6j, IMF B_y was indeed large and negative during the second flow reversal, and IMF B_z was weaker and positive.

5. Thermal Properties as Indicator of Reconnection

Plate 3b shows that the tailward flowing plasma is much hotter than the earthward flowing plasma. The abrupt temperature jumps across the flow reversals may indicate that the plasma on the two sides of the flow reversals is not magnetically connected, as expected for plasma on two sides of an X line. The reason for the tailward flowing plasma being hotter is presently not understood.

6. Summary and Conclusion

We have analyzed in detail a 10 hour interval of high-speed convective plasma flows encountered by the Wind spacecraft at $X_{GSE} \sim -60\ R_E$. Both earthward and tailward flows were detected during this interval. The hypothesis that these high-speed flows are produced by reconnection has been tested using variance and Walén analyses. The main findings can be summarized as follows:

1. Six intervals of high-speed flows (in both the earthward and tailward directions) where a good deHoffmann-Teller frame could be found were chosen for Walén analysis case studies. For all intervals the flow velocity in the deHoffmann-Teller frame of reference was found to be well correlated with the Alfvén velocity. The velocity in the deHoffmann-Teller frame was found to be between 52% and 83% of the Alfvén speed for all cases, except for one tailward flow case where the slope was only 33%. The sub-Alfvénic flow is expected for slow shocks in tail reconnection [*Hau and Sonnerup*, 1989]. The sign of the Walén slope is related to the sense of the flow, according to the prediction of reconnection (Figure 2). Such a systematic relation is not trivial and cannot be explained by random propagation of Alfvén or slow-mode waves.

2. To demonstrate that the six events chosen for the case studies were not atypical, the same analysis was performed

on the whole 10 hour interval, using a sliding window of 12 min duration. Similar results were obtained from the Walén test, and the average flow speed was 57% of the Alfvén speed.

3. The variance analyses on the magnetic field, the electric field, and the Faraday residue indicate a large tilt (40°-61°) of the neutral sheet during the high-speed flow interval. The sense of the tilt is consistent with the dominant negative IMF B_y component during the event.

4. The variance analysis shows that the component of the magnetic field normal to the neutral sheet switches sign near the flow reversals, consistent with the passage of an X line.

5. The large temperature difference between the earthward and tailward flowing plasmas suggests that the plasmas on the two sides of the flow reversal are not magnetically linked, a feature that would also be consistent with reconnection.

6. The high-speed flows analyzed in detail here (Plate 3) occurred during an interval of low geomagnetic activity ($Kp < 2$) and northward IMF orientation. Whether localized activity in the auroral zone occurred during these times requires further investigation.

In summary, the Walén test, the variance analysis, and the thermal properties of the plasma all give results consistent with the simple picture depicted by Figure 2. Together, these analyses provide evidence for earthward and tailward high-speed jets originating from a reconnection site near X_{GSE} =-60 R_E. Thus our observations imply that quasi-steady reconnection can occur in the midmagnetotail during steady northward IMF.

For the ~10 hour interval of high-speed flows studied in detail here (Plate 3) the earthward high-speed flow precedes the tailward high-speed flow, indicating that the X line was formed at a distance tailward of $X_{GSE} \sim -60\ R_E$, and then moved earthward. However, after ~2 hours of tailward flow, another flow reversal occurred, and the direction of the high-speed flow changed back to earthward. This change in flow direction suggests that the X line now retrieved tailward. However, it cannot be ruled out that the two flow reversals were due to the motion of two independent X lines. This question cannot be resolved with a single spacecraft.

The long-duration high-speed flows reported in this study are in contrast to bursty bulk flows (BBFs) detected in the near-Earth plasma sheet. The BBFs are typically short lived and have been suggested to be produced by near-Earth (~20-30 R_E downtail) reconnection [e.g., *Baumjohann et al.*, 1989, 1990; *Angelopoulos et al.*, 1992; Nagai et al., 1998]. BBFs have been linked to the onset of auroral activity, whereas the present long-duration high-speed flows occurred during quiet times. It should be mentioned that long-duration high-speed flows are not uncommon in the midtail [e.g., *Troshichev et al.*, 1999] and the distant tail [e.g., *Nishida et al.*, 1995] plasma sheet. The relationship between the long-duration fast flows in the midtail (40-80 R_E) region and the shorter-duration BBFs still needs to be investigated.

Acknowledgments. We would like to thank Ron Lepping, the principal investigator of the Wind magnetic field experiment, and the ACE MAG experiment teams for making their data available. We are grateful to Forrest Mozer and Masaki Fujimoto for helpful discussions. We thank Stan Cowley, Götz Paschmann, and Jim Slavin for their comments on the manuscript. This research was funded in part by NASA grant FDNAG5-6928 at U. C. Berkeley and NASA grant NAG5-7185 at Dartmouth College.

Hiroshi Matsumoto thanks A. Nishida and D. G. Sibeck for their assistance in evaluating this paper.

References

Angelopoulos, V., W. Baumjohann, C. F. Kennel, F. V. Coroniti, M. G. Kivelson, R. Pellat, R. J. Walker, H. Lühr, and G. Paschmann, Bursty bulk flows in the inner central plasma sheet, *J. Geophys. Res., 97*, 4027, 1992.

Baumjohann, W., G. Paschmann, and C. Catell, Average plasma properties in the central plasma sheet, *J. Geophys. Res., 94*, 6597, 1989.

Baumjohann, W., G. Paschmann, and H. Lühr, Characteristics of high-speed ion flows in the plasma sheet, *J. Geophys. Res., 95*, 3801, 1990.

Cowley, S. W. H., Magnetospheric asymmetries associated with the y-component of the IMF, *Planet. Space Sci., 29*, 79, 1981.

Dungey, J. W., Interplanetary magnetic field and the auroral zones, *Phys. Rev. Lett., 6*, 47, 1961.

Feldmann, W. C., et al., Evidence for slow-mode shocks in the deep geomagnetic tail, *Geophys. Res. Lett., 11*, 599, 1984.

Feldmann, W. C., D. N. Baker, S. J. Bame, J. Birn, J. T. Gosling, E. W. Hones Jr., and S. J. Schwartz, Slow-mode shocks: A semipermanent feature of the distant geomagnetic tail, *J. Geophys. Res., 90*, 233, 1985.

Gosling, J. T., M. F. Thomsen, S. J. Bame, and C. T. Russel, Accelerated plasma flows at the near-tail magnetopause, *J. Geophys. Res., 91*, 3029, 1986.

Gosling, J. T., M. F. Thomsen, S. J. Bame, R. C. Elphic, and C. T. Russell, Plasma flow reversals at the dayside magnetopause and the origin of asymmetric polar cap convection, *J. Geophys. Res., 95*, 8073, 1990.

Hau, L.-N., and B. U. Ö. Sonnerup, On the structure of resistive MHD intermediate shocks, *J. Geophys. Res., 94*, 6539, 1989.

Kawano, H., and T. Higuchi, A generalization of the minimum variance analysis method, *Ann. Geophys., 14*, 1019, 1996.

Khrabrov, A. V., and B. U. Ö. Sonnerup, DeHoffmann-Teller analysis, in *Analysis Methods for Multi-Spacecraft Data*, edited by G. Paschmann and P. W. Daly, *ISSI Sci. Rep. SR-001*, Eur. Space Agency Publ. Div., Noordwijk, Netherlands, 1998a.

Khrabrov, A. V., and B. U. Ö. Sonnerup, Orientation and motion of current layers: Minimization of the Faraday residue, *Geophys. Res. Lett., 25*, 2373, 1998b.

Lepping, R. P., et al., The Wind magnetic field investigation, *Space Sci. Rev., 71*, 207, 1995.

Levy, R. H., H. E. Petschek, and G. L. Siscoe, Aerodynamic aspects of the magnetospheric flow, *AIAA, 2*, 2065, 1964.

Lin, R. P., et al., A three-dimensional plasma and energetic particle investigation for the Wind spacecraft, *Space Sci. Rev., 71*, 125, 1995.

Maezawa, K., T. Hori, Y. Saito, T. Mukai, T. Yamamoto, S. Kokobun, and A. Nishida, Structure of the distant magnetotail and its dependence on the IMF B_y component, *Adv. Space Res., 20*, 949, 1997.

Nagai, T., M. Fujimoto, Y. Saito, S. Machida, T. Terasawa, R. Nakamura, T. Yamamoto, T. Mukai, A. Nishida, and S. Kokobun, Structure and dynamics of magnetic reconnection for substorm onsets with Geotail observations, *J. Geophys. Res., 103*, 4419, 1998.

Nishida, A., T. Mukai, T. Yamamoto, Y. Saito, S. Kokobun, and K. Maezawa, Geotail observations of magnetospheric convection in the distant tail at 200 R_E in quiet times, *J. Geophys. Res., 100*, 23,663, 1995.

Paschmann, G., B. U. Ö. Sonnerup, I. Papamastorakis, N. Sckopke, G. Haerendel, S. J. Bame, J. R. Asbridge, J. T. Gosling, C.

T. Russell, and R. C. Elphic, Plasma acceleration at the Earth's magnetopause: Evidence for reconnection, *Nature, 282*, 243, 1979.

Paschmann, G., I. Papamastorakis, W. Baumjohann, N. Sckopke, C. W. Carlson, B. U. Ö. Sonnerup, and H. Lühr, The magnetopause for large magnetic shear: AMPTE/IRM observations, *J. Geophys. Res., 91*, 11,099, 1986.

Petschek, H. E., Magnetic field annihilation, in *AAS-NASA Symposium on Solar Flares, NASA Spec. Publ. SP-50*, 425, 1964.

Richardson, I. G., C. J. Owen, S. W. H. Cowley, A. B. Galvin, T. R. Sanderson, M. Scholer, J. A. Slavin, and R. D. Zwickl, ISEE 3 observations during the CDAW 8 intervals: Case studies of the distant geomagnetic tail covering a wide range of geomagnetic activity, *J. Geophys. Res., 94*, 15,189, 1989.

Saito, Y., T. Mukai, T. Terasawa, A. Nishida, S. Machida, M. Hirahara, K. Maezawa, S. Kokobun, and T. Yamamoto, Slow-mode shocks in the magnetotail, *J. Geophys. Res, 100*, 23,567, 1995.

Seon, J., L. A. Frank, W. R. Paterson, J. D. Scudder, F. V. Coroniti, S. Kokobun, and T. Yamamoto, Observations of slow-mode shocks in Earth's distant magnetotail with the Geotail spacecraft, *J. Geophys. Res, 101*, 27,383, 1996.

Sibeck, D. G., G. L. Siscoe, J. A. Slavin, E. J. Smith, B. T. Tsurutani, and R. P. Lepping, The distant magnetotail's response to a strong interplanetary magnetic field B_y: Twisting, flattering, and field line bending, *J. Geophys. Res, 90*, 4011, 1985.

Sonnerup, B. U. Ö., and L. J. Cahill. Jr., Magnetopause structure and attitude from Explorer 12 observations, *J. Geophys. Res., 72*, 171, 1967.

Sonnerup, B. U. Ö., G. Paschmann, I. Papamastorakis, N. Sckopke, G. Haerendel, S. J. Bame, J. R. Asbridge, J. T. Gosling, and C. T. Russell, Evidence for magnetic reconnection at the Earth's magnetopause, *J. Geophys. Res., 86*, 10,049, 1981.

Sonnerup, B. U. Ö., I. Papamastorakis, G. Paschmann, and H. Lühr, Magnetopause properties from AMPTE/IRM observations of the convection electric field: Method development, *J. Geophys. Res., 92*, 12,137, 1987.

Sonnerup, B. U. Ö., I. Papamastorakis, G. Paschmann, and H. Lühr, The magnetopause for large magnetic shear: Analysis of convection electric field from AMPTE/IRM, *J. Geophys. Res., 95*, 10,541, 1990.

Sonnerup, B. U. Ö., G. Paschmann, and T. D. Phan, Fluid aspects of reconnection at the magnetopause: In situ observations, in *Physics of the Magnetopause, Geophys. Monogr. Ser.*, vol. 90, edited by P. Song, B. U. Ö. Sonnerup, M. F. Thomsen, pp. 167-180, AGU, Washington, D. C., 1995.

Terasawa, T., et al., On the determination of a moving MHD structure: Minimization of the residue of integrated Faraday's equation, *J. Geomagn. Geoelectr., 48*, 603, 1996.

Troshichev, O. A., S. Kokobun, Y. Kamide, T. Mukai, and T. Yamamoto, Fast earthward plasma flows observed in the mid/distant tail under quiet conditions: Relation to substorms, *Geophys. Res. Lett., 26*, 643, 1999.

R. P. Lin, M. Øieroset, T.-D. Phan, Space Sciences Laboratory, University of California, Berkeley, CA 94720. (oieroset@ssl.berkeley.edu)

B. U. Ö. Sonnerup, Dartmouth College, Thayer School Engineering, 8000 Cummings Hall, Hanover, NH 03755-8000 (bengt.u.o.sonnerup@dartmouth.edu)

(Received February 1, 2000; revised April 13, 2000;
accepted May 18, 2000.)